Eigenvalue repulsion in an effective theory of SU(2) Wilson lines in three dimensions

Adrian Dumitru and Dominik Smith

Institut für Theoretische Physik, Johann Wolfgang Goethe-Universität, Max-von-Laue-Str. 1, 60438 Frankfurt am Main, Germany

(Received 14 November 2007; published 27 May 2008)

We perform simulations of an effective theory of SU(2) Wilson lines in three dimensions. We include a nonperturbative "fuzzy-bag" contribution, which is added to the one-loop perturbative potential for the Wilson line. We confirm that, at moderately weak coupling, this leads to eigenvalue repulsion in a finite region above the deconfining phase transition, which shrinks in the extreme weak-coupling limit. A nontrivial $Z(N)$ symmetric vacuum arises in the confined phase.

DOI: 10.1103/PhysRevD.77.094022 PACS numbers: 12.38.−t, 12.38.Gc, 12.38.Mh

I. INTRODUCTION

In QCD at very high temperature, the pressure is due to weakly interacting quasiparticle gluons. (Here, we ignore contributions from quarks and focus on the pure gauge theory.) It can be calculated from an effective theory in three dimensions[1]

$$\mathcal{L}^{\text{eff}} = \tfrac{1}{2}\mathrm{tr}G_{ij}^2 + \mathrm{tr}|D_iA_0|^2 + m_D^2\mathrm{tr}A_0^2 + \cdots; \qquad (1)$$

see [1,2] and references therein. G_{ij} is the magnetic field strength associated with the spatial components of the vector potential $\boldsymbol{A}$, m_D is the Debye mass, and the dots represent self interactions of A_0. The effective theory (1) is valid as long as fluctuations in A_0 are small; that is, the expectation value of the Polyakov loop in the original four-dimensional theory, which is given by the trace of the thermal Wilson line,

$$\ell(\boldsymbol{x}) = \frac{1}{N}\,\mathrm{tr}\mathbf{L}(\boldsymbol{x}), \qquad (2)$$

$$\mathbf{L}(\boldsymbol{x}) = \mathcal{Z}_R^{-1}\mathcal{P}\exp\left(ig\int_0^{1/T} d\tau A_0(\boldsymbol{x},\tau)\right), \qquad (3)$$

should be close to one of the N roots of unity, where N is the number of colors. We have indicated explicitly that in the four-dimensional theory, $A_0(\boldsymbol{x},\tau)$ depends on Euclidean time τ, and that Polyakov loops have to be renormalized to obtain a nonzero continuum limit [3,4]. The renormalization constant $\mathcal{Z}_R$ depends on the representation of $\mathbf{L}$, taken here to be the fundamental representation; thus, $\mathbf{L}$ represents the propagator of an infinitely heavy test quark. Also, we always consider normalized traces and divide by the dimension of the representation.

The Polyakov loop represents an order parameter for the spontaneous breaking of the global $Z(N)$ center symmetry corresponding to gauge transformations that are periodic in τ only up to an element of $Z(N)$. In the high-temperature deconfined phase, the Polyakov loop acquires a nonvanishing expectation value but vanishes in the confined phase [5]. As a consequence of the $Z(N)$ symmetry in the original four-dimensional theory, when A_0/T is large (of order $1/g$), the effective electric field in three dimensions is not simply $E_i(\boldsymbol{x}) = D_i(\boldsymbol{x})A_0(\boldsymbol{x})$ [1,6].

For two colors, the phase transition is of second order [7,8] and so, $\langle\ell\rangle(T_d) = 0$ vanishes continuously (the theory is in the $Z(2)$ universality class [9]). Hence, in the immediate vicinity of T_d at least, the Polyakov loop is clearly far from unity. For $N = 3$, the transition is first order [10] and $\langle\ell\rangle$ is discontinuous at T_d. If the SU(3) gluon plasma was perturbative all the way down to T_d^+ [in the electric sector, $\langle\ell\rangle(T_d^+) \approx 1$], then (1) *might* have applied even for T just above T_d. However, lattice measurements [3,4] indicate that $\langle\ell\rangle(T_d^+) \lesssim 0.5$, which is rather far from unity. Moreover, the ratio of screening masses defined from two-point correlation functions of the real and the imaginary part of the Polyakov loop, respectively, increases from $\approx 3{:}2$ (which is the LO result from perturbation theory) at high temperature to ≈ 3 near T_d [11]. Also, resummations of perturbation theory work very well at high T but appear to fail to reproduce the pressure or the entropy density [12] below $\approx 3T_d$. Finally, the interaction measure $(e - 3p)/T^4$ for both two [7] and three [10] colors is rather large up to $T \approx 3T_d$.

These observations may suggest that at temperatures not very far above T_d, that even at weak coupling, the theory is nonperturbative in the sense that A_0/T is large. If so, it is useful then to construct an effective theory in terms of the Wilson line $\mathbf{L}$ rather than A_0 [1,2,13,14]. This Lagrangian can also incorporate the global $Z(N)$ symmetry for the Polyakov loop.

As shown in Ref. [1], the electric field in the three-dimensional theory for *arbitrary* A_0 is given by

$$E_i(\boldsymbol{x}) = \frac{T}{ig}\mathbf{L}^\dagger(\boldsymbol{x})D_i(\boldsymbol{x})\mathbf{L}(\boldsymbol{x}). \qquad (4)$$

The classical Lagrangian in three dimensions then becomes

[1]That is, all fields in (1) are functions of $\boldsymbol{x}$ only, and the action is given by an integral of the Lagrangian over space, divided by temperature.

$$\mathcal{L}^{\rm eff}_{\rm cl} = \frac{1}{2}\,{\rm tr}G_{ij}^2 + \frac{T^2}{g^2}\,{\rm tr}|\mathbf{L}^\dagger D_i \mathbf{L}|^2. \tag{5}$$

Contrary to sigma models with left-right symmetry, for loops there is also a potential. It can be written as an infinite sum over all $Z(N)$ neutral loops [15]. For the present purposes, however, we rather write it in terms of powers of the fundamental Wilson line. To one loop and for constant $\mathbf{L}$, [16]

$$\mathcal{L}^{\rm eff}_{1-{\rm loop}} = -\frac{2}{\pi^2}T^4\sum_{n\geq 1}\frac{1}{n^4}|{\rm tr}\mathbf{L}^n|^2. \tag{6}$$

This potential is evidently minimized by the perturbative vacuum $\langle \mathbf{L}\rangle = \mathbb{1}$ (times a phase), for any T. To generate a phase transition in infinite volume, Ref. [1] suggested to add nonperturbative contributions, such as

$$\mathcal{L}^{\rm eff}_{\rm non-pert} = B_f T^2 |{\rm tr}\mathbf{L}|^2, \tag{7}$$

with B_f a ''fuzzy-bag'' constant (see, also, Refs. [17,18]). At sufficiently low temperature, (7) dominates over the perturbative potential (6) and induces a transition to a confined phase with $\langle {\rm tr}\mathbf{L}\rangle = 0$. It was further suggested in [1] that terms such as (7) lead to ''repulsion'' of the eigenvalues of the Wilson line in some temperature range above T_d. If so, then the distribution of eigenvalues should deviate from a sharp peak near 1 for nonasymptotic temperatures. Our numerical results confirm this idea in the regime where the nearest-neighbor coupling $\beta \sim 1/g^2$ is not so large as to suppress fluctuations of the Wilson lines in space.

In this paper, we perform Monte Carlo simulations of an effective theory motivated by (5)–(7) on a three-dimensional lattice. The theory is defined with a spatial cutoff on the order of the inverse temperature as (5) is nonrenormalizable in three dimensions and is valid only over distance scales larger than $1/T$.[2] We shall focus, in particular, on measuring the eigenvalue distribution both above and at the (de-)confining phase transition, thereby testing the presence of eigenvalue repulsion in the phase transition region. We presently employ several approximations that simplify the simulations drastically. Most importantly, the present simulations neglect the magnetic sector

$$A_i = 0. \tag{8}$$

Hence, the gauge theory is essentially reduced to a sigma model. A precise matching of the couplings in the effective theory to correlation functions measured in the continuum limit of the original four-dimensional theory is beyond the scope of this paper. Furthermore, we neglect all but the $n = 1$ term in (6), which can then be combined with the nonperturbative potential (7).

It should be noted, in particular, that the matrix model studied below is in a different universality class than four-dimensional SU(2) Yang-Mills theory (for a recent discussion of the latter, see Ref. [8]). Therefore, near the transition, long-distance properties will not match. Nevertheless, we introduce (9) here as a simple realization of a matrix model that allows us to study the distribution of eigenvalues of $\mathbf{L}$ in the plane of nearest-neighbor matrix coupling β and fuzzy-bag constant (or temperature) m^2.

II. THE LATTICE ACTION

Our general three-dimensional lattice action includes kinetic (nearest-neighbor interaction) and mass terms

$$\mathcal{S} = -\frac{1}{2}\beta\sum_{\langle ij\rangle}{\rm tr}(\mathbf{L}_i\mathbf{L}_j^\dagger + {\rm H.c.}) - m^2\sum_i |{\rm tr}\mathbf{L}_i|^2, \tag{9}$$

where $\mathbf{L}$ denotes SU(2) Wilson lines in the fundamental representation, i labels sites, and $\langle ij\rangle$ labels links. We employ periodic boundary conditions. The kinetic term is invariant under global ${\rm SU}_L(2)\times{\rm SU}_R(2)$ transformations, while the mass term breaks it to SU(2). The weak-coupling limit of the original four-dimensional theory corresponds to large β. The partition function involves an integral over the invariant SU(2) measure $[d\mathbf{L}]$ at each site,

$$\mathcal{Z} = \int\prod_n [d\mathbf{L}_n] e^{-\mathcal{S}}. \tag{10}$$

III. MEAN-FIELD APPROXIMATION

The mean-field approximation for the matrix model has been discussed in detail in Refs. [4,15,20,21]. We briefly review the main steps and results as required for our present purposes.

Replace all $2d$ nearest neighbors of any given site in (9) by a fixed matrix $\bar{\mathbf{L}}$, where $d = 3$ is the number of spatial dimensions. This defines a single-site free energy

$$e^{-N_s^d\mathcal{F}_{ss}(\bar{\mathbf{L}})} = \mathcal{Z}_{ss}^{N_s^d}, \tag{11}$$

where N_s is the number of sites per spatial dimension and

$$\mathcal{Z}_{ss} = \int[d\mathbf{L}]\exp[d\beta\,{\rm tr}(\mathbf{L}\bar{\mathbf{L}}^\dagger + {\rm H.c.}) + m^2|{\rm tr}\mathbf{L}|^2]. \tag{12}$$

Consistency requires that

$$\langle(\mathbf{L})^*_{lk}\rangle = \frac{1}{d\beta}\frac{\partial}{\partial(\bar{\mathbf{L}})_{lk}}\log\mathcal{Z}_{ss}(\bar{\mathbf{L}}) \tag{13}$$

be equal to

$$(\bar{\mathbf{L}})^*_{lk} = \frac{\partial}{\partial(\bar{\mathbf{L}})_{lk}}(\bar{\mathbf{L}})^*_{lk}(\bar{\mathbf{L}})_{lk}. \tag{14}$$

[2]A related renormalizable theory has been formulated in Refs. [2,13]. Reference [19] derived the relations between lattice and continuum theories to leading order in lattice perturbation theory.

It follows that $\bar{\mathbf{L}}$ minimizes a mean-field free energy defined as

$$0 = \frac{\partial}{\partial \bar{\mathbf{L}}} \mathcal{F}_{\rm mf}(\bar{\mathbf{L}}), \tag{15}$$

$$\mathcal{F}_{\rm mf}(\bar{\mathbf{L}}) = \mathcal{F}_{ss}(\bar{\mathbf{L}}) + d\beta\, {\rm tr}\bar{\mathbf{L}}^\dagger \bar{\mathbf{L}}. \tag{16}$$

To proceed, we assume that $\bar{\mathbf{L}}$ is proportional to the unit matrix, $\bar{\mathbf{L}} = \bar{\ell}\mathbb{1}$ (for two colors, $\bar{\ell}$ can be chosen to be real), so that

$$e^{-\mathcal{F}_{ss}(\bar{\ell})} = \int [d\mathbf{L}] \exp[2d\beta\bar{\ell}\,{\rm tr}(\mathbf{L} + \mathbf{L}^\dagger) + m^2 |{\rm tr}\mathbf{L}|^2]. \tag{17}$$

The action is a function only of the trace of the integration variable, so that we can write

$$\mathbf{L} = \exp {\rm diag}(i\phi, -i\phi + 2\pi i n), \tag{18}$$

with n an arbitrary integer, and employ Weyl's parameterization

$$[d\mathbf{L}] \sim d\phi |\Delta(\phi)|^2 = d\phi \sin^2\phi, \tag{19}$$

where $\Delta(\phi)$ denotes the Vandermonde determinant. Up to an overall constant then,

$$e^{-\mathcal{F}_{ss}(\bar{\ell})} = \int_{-1}^{1} d\cos\phi \exp\Big[4d\beta\bar{\ell}\cos\phi + 4m^2\cos^2\phi + \frac{1}{2}\log(1-\cos^2\phi)\Big]. \tag{20}$$

This integral could now be evaluated analytically in a saddle-point approximation. However, we have found that for $d = 3$, the analytical result is too inaccurate to be useful in practice, in particular, in the interesting region of β and m^2. Therefore, we have rather tabulated (20) as a function of $\bar{\ell}$. The expectation value ℓ_0 of ${\rm tr}\mathbf{L}/2$ is then given by the location of the minimum of

$$\mathcal{F}_{\rm mf}(\bar{\ell}) = \mathcal{F}_{ss}(\bar{\ell}) + 2d\beta\bar{\ell}^2. \tag{21}$$

IV. RESULTS

A. The model with global $SU_L(2) \times SU_R(2)$ symmetry

We begin with the pure nearest-neighbor interaction model with no *loop potential*, corresponding to Eqs. (9) and (10), with $m^2 = 0$ [20]:

$$\mathcal{S} = -\frac{1}{2}\beta \sum_{\langle ij\rangle} {\rm tr}(\mathbf{L}_i \mathbf{L}_j^\dagger + {\rm H.c.}). \tag{22}$$

Note that in (22) the basic degrees of freedom are the Wilson line matrices, or their eigenvalues; the model therefore differs from others that deal exclusively with the trace of $\mathbf{L}$ such as $\mathcal{S} \sim -\beta\sum({\rm tr}\mathbf{L}_i\, {\rm tr}\mathbf{L}_j^\dagger + {\rm c.c.})$ [22]. Alternatively, one may consider nearest-neighbor interactions between Polyakov loops in arbitrary representations [4,15,23].

We expect that for small β there is a phase where the adjoint fields

$$\tilde{\ell}^{\,a}(\boldsymbol{x}) = \frac{1}{2i}\,{\rm tr}\mathbf{L}(\boldsymbol{x})\boldsymbol{\tau}^{\boldsymbol{a}} \tag{23}$$

as well as the singlet field (which is actually the Polyakov loop)

$$\ell(\boldsymbol{x}) = \tfrac{1}{2}{\rm tr}\mathbf{L}(\boldsymbol{x}) \tag{24}$$

are massive.[3] Furthermore, the expectation value of the "length" of $\bar{\mathbf{L}}$,

$$u = \sqrt{{\rm tr}\bar{\mathbf{L}}^\dagger\bar{\mathbf{L}}/2}, \qquad u_0 = \langle u\rangle, \tag{25}$$

should vanish also. The bar stands for the average over the volume for any given configuration:

$$\bar{\mathbf{L}} = \frac{1}{N_s^3}\sum_i \mathbf{L}_i, \tag{26}$$

while $\langle\cdot\rangle$ is the average over configurations. Note that ${\rm tr}\bar{\mathbf{L}}^\dagger\bar{\mathbf{L}}/2 = 2({\rm tr}\bar{\mathbf{L}}/2)^2 - {\rm tr}\bar{\mathbf{L}}^2/2 \equiv \bar{\ell}^2 - \bar{\ell}_2$, where ℓ_2 is the Polyakov loop with $Z(N)$ charge two [24] (which is neutral when $N = 2$).

For sufficiently large β, on the other hand, the Wilson lines at different sites have to align in order to minimize the action (22). Hence, for a given configuration (resp. Metropolis time) $\bar{\mathbf{L}}$ should be nonzero. However, its direction in group space will rotate from configuration to configuration, implying $\langle\bar{\mathbf{L}}\rangle = 0$. To monitor the transition to an ordered phase at large β, we therefore use $\langle u\rangle$ rather than $\langle{\rm tr}\bar{\mathbf{L}}\rangle$ as order parameter [20]. Alternatively, one could add a weak background field $-h\,{\rm tr}\mathbf{L}$, which is then taken to zero after the extrapolation to infinite volume has been performed.

The regimes where $\langle u\rangle = 0$ and $\langle u\rangle \neq 0$, respectively, are separated by a second-order phase transition at some critical β_c [20], which we determine numerically. This transition is associated with spontaneous breaking of the $SU_L(2) \times SU_R(2)$ symmetry to $SU_V(2)$, where three Goldstone modes appear.

The ensemble average denoted by $\langle\cdot\rangle$ should be performed over statistically independent configurations. It is therefore necessary to determine the autocorrelation time of the Monte Carlo algorithm as a function of β. This is done via the "rebinning method" [25] as follows. First, we group the sequence $\mathcal{O}_i$ of measurements of a given operator[4] into N_{bs} bins of size N_b,

[3] We assume Hermitian generators normalized according to ${\rm tr}\boldsymbol{\tau}^{\boldsymbol{a}}\boldsymbol{\tau}^{\boldsymbol{b}} = 2\delta^{ab}$.

[4] We take $\mathcal{O} = u$ defined in Eq. (25).

$$\mathcal{O}_j(N_b) = \frac{1}{N_b} \sum_{i=jN_b}^{(j+1)N_b-1} \mathcal{O}_i, \tag{27}$$

where $j = 0 \cdots N_{bs} - 1$ labels the bins. Hence, $\mathcal{O}_j(N_b)$ is simply the mean over the measurements belonging to the bin j. We then determine the variance of the new sequence $\mathcal{O}_j(N_b)$

$$\sigma^2_{N_b} = \frac{1}{N_{bs}} \sum_{j=0}^{N_{bs}-1} (\mathcal{O}_j(N_b) - \langle \mathcal{O} \rangle)^2. \tag{28}$$

$\langle \mathcal{O} \rangle$ denotes the average of $\mathcal{O}$ over all configurations. The integrated autocorrelation time corresponding to the bin-size N_b is given by

$$\tau_{\text{int}}(N_b) = \frac{\sigma^2_{N_b}}{\sigma^2}, \tag{29}$$

where σ^2 denotes the variance of the original sequence of measurements. We then plot $\tau_{\text{int}}(N_b)$ versus N_b, which eventually approaches a flat plateau (up to rapid oscillations). This defines τ_{int}, which is shown in Fig. 1 as a function of β. In the vicinity of the critical point, the Metropolis update algorithm displays the well-known critical slowing down phenomenon; τ_{int} diverges in the infinite-volume limit. The measurements obtained on $N_s = 24$, 36, 48 lattices can be fitted with the form $\tau_{\text{int}} \sim N_s^{1/\nu_\tau}$, with the scaling exponent

$$\nu_\tau = 0.72(4). \tag{30}$$

Away from β_c, the autocorrelation time decreases. Notice, however, that it increases with the volume even above the critical point, while it exhibits the standard behavior for $\beta < \beta_c$.

In practice, our simulations are performed as follows. The initial configuration of SU(2) matrices is chosen randomly. We then perform a number of thermalization steps, which is larger than the autocorrelation time τ_{int} (determined beforehand in a prerun) of the order parameter. Subsequently, measurements are performed in time intervals slightly larger than τ_{int}. We employ a standard Metropolis update [25], where all N_s^3 sites are scanned in sequence. Typically, we summed on the order of a thousand configurations for each set of couplings.

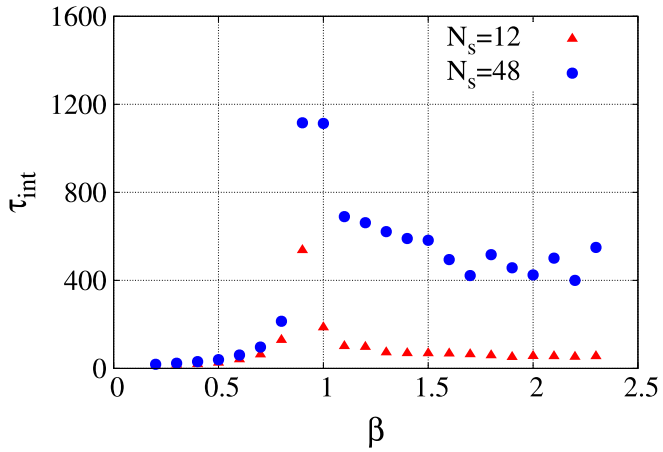

FIG. 1 (color online). The integrated autocorrelation time as a function of the coupling β for various lattices.

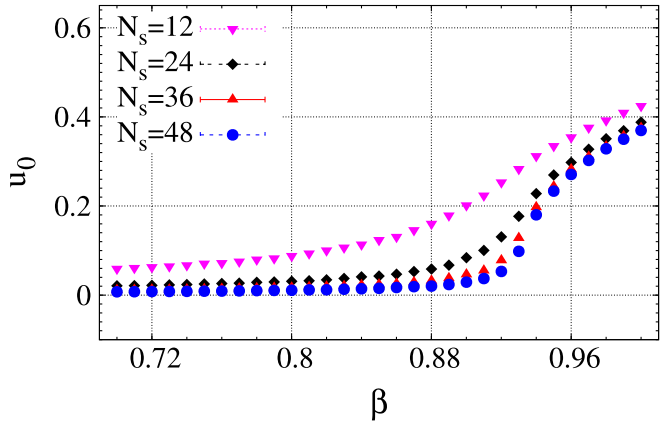

FIG. 2 (color online). The length of the $O(4)$-like order parameter from Eq. (25) as a function of the coupling β for various lattices.

Figure 2 shows the expectation value of the order parameter (25) as a function of β on lattices of various sizes. Statistical error bars are smaller than the size of the symbols. There is, clearly, a order-disorder transition at $\beta_c \simeq 0.9$. As expected, finite-size effects are visible around the transition point ($\beta \simeq \beta_c$). We have verified that u_0 approaches 1 for $\beta \gg 1$.

To estimate the infinite-volume limit of β_c, we proceed as follows. We first determine the temperature susceptibility $\chi(\beta) = \partial u_0 / \partial \beta$, as shown in Fig. 3. The location of the maximum defines β_c for any given lattice size. Extrapolating linearly to $1/N_s = 0$, we obtain

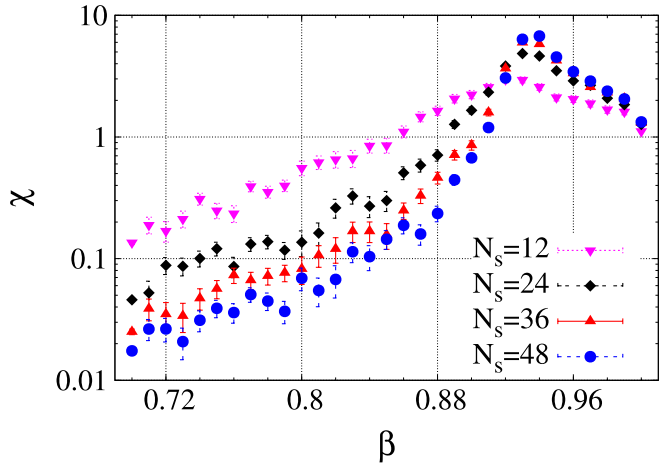

FIG. 3 (color online). The derivative of the order parameter from Eq. (25) with respect to β as a function of the coupling β on various lattices.

$$\beta_c = 0.942(5). \tag{31}$$

We have verified that the derivative of the average kinetic energy per link $E \sim \mathrm{Re}\langle \mathrm{tr}\mathbf{L}_i^\dagger \mathbf{L}_{i+1}\rangle$ with respect to β also peaks at the same value of the coupling, which is somewhat larger than the estimate from Ref. [20], who employed smaller lattices and lower statistics.

In Fig. 4 we show two time sequences for the Polyakov loop just below and far above β_c. It is clear that below the phase transition, there are only small fluctuations about 0, which decrease on larger lattices. On the other hand, at large β, the Wilson lines partly align and $|\bar{\ell}|$ is far from 0 for long time intervals. However, the above-mentioned slow rotation of $\bar{\mathbf{L}}$ in group space (in the absence of a background field) is clearly visible. We emphasize that Fig. 4 depicts two particular runs that were much shorter than those used for measurement.

Next, we consider two-point matrix-matrix correlation functions of the form

$$\mathcal{C}_{\mathbf{L}}(r) = \frac{1}{3}\frac{1}{N_s^3}\sum_{\hat{r},\boldsymbol{r}_0}\frac{1}{2}\langle \mathrm{tr}\mathbf{L}^\dagger(\boldsymbol{r}_0)\mathbf{L}(\boldsymbol{r}_0+\boldsymbol{r})\rangle. \tag{32}$$

The vector $\boldsymbol{r}$ is allowed to point in any of the three principal directions of the lattice (in the positive direction only), over which we average. Also, its length is restricted to $< N_s/2$ due to the periodic boundary conditions.

Having determined the two-point function $\mathcal{C}(r)$ and its statistical error, we perform a χ^2 fit to the functional form

$$\mathcal{C}_{\mathbf{L}}(r) \sim \frac{1}{r m_\xi} e^{-r m_\xi} + \mathrm{const} \tag{33}$$

to extract the inverse spatial correlation length m_ξ. The fits were restricted to $r \geq 4$ (in lattice units) such that $\chi^2/\mathrm{dof} \simeq 1$.

Figure 5 displays $m_\xi(\beta)$ for lattices of various sizes. Deep in the disordered phase, correlations extend only over a few lattice sites, and m_ξ is therefore independent of the volume. This confirms that both the $\tilde{\ell}^a$ and the Polyakov loop ℓ are massive. Long-range correlations do develop near β_c, and m_ξ drops to nearly zero, up to finite-size effects. A fit of the form $m_\xi(\beta_c) \sim N_s^{-1/\nu_\xi}$ ($N_s = 24$, 36, 48 lattices only) gives the scaling exponent

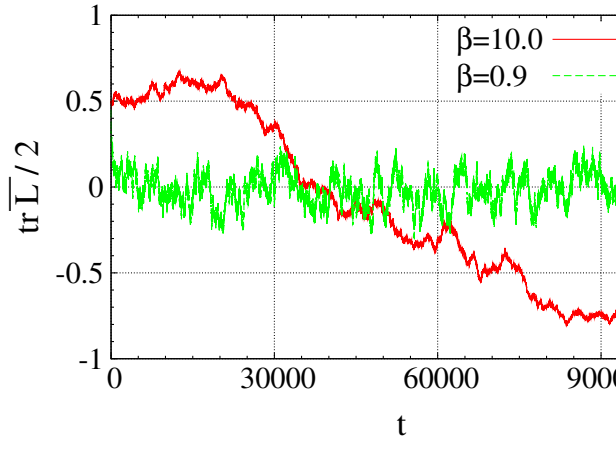

FIG. 4 (color online). Time evolution of the volume-averaged Polyakov loop below and far above β_c; $N_s = 12$ lattice.

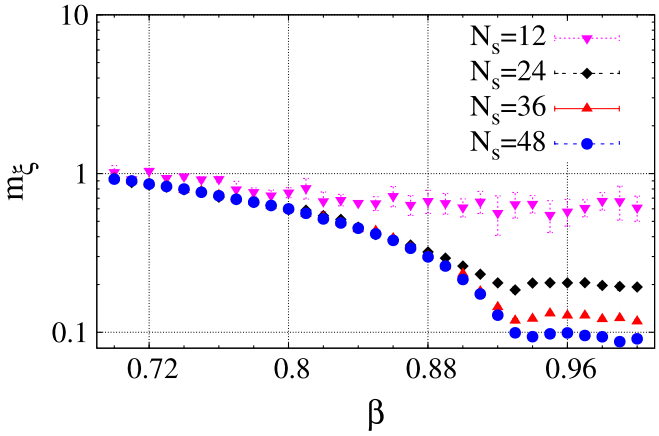

FIG. 5 (color online). The inverse spatial correlation length as a function of the coupling β for various lattices.

$$\nu_\xi = 0.938(5). \tag{34}$$

Quite clearly, there are massless modes (again, up to finite-size effects) even above β_c, and hence m_ξ remains small. These observations are in line with the behavior of the integrated autocorrelation time τ_{int} for $\beta > \beta_c$ mentioned above. We have also measured the correlation lengths for Polyakov loops and for the adjoint $\tilde{\ell}^a$ fields via fits of the form (33) to the two-point functions

$$\mathcal{C}_\ell(r) \sim \sum_{\hat{r},\boldsymbol{r}_0}\langle \ell(\boldsymbol{r}_0)\ell(\boldsymbol{r}_0+\boldsymbol{r})\rangle, \tag{35}$$

$$\mathcal{C}_{\tilde{\ell}}(r) \sim \sum_{\hat{r},\boldsymbol{r}_0}\langle \tilde{\ell}(\boldsymbol{r}_0)\cdot\tilde{\ell}(\boldsymbol{r}_0+\boldsymbol{r})\rangle. \tag{36}$$

We refrain from showing the results here, since they closely resemble $m_\xi(\beta)$ from Fig. 5. The fact that the correlation length for ℓ appears to diverge even above β_c is probably due to mixing with the Goldstone modes.

Finally, we determine the distribution of eigenvalues of the Wilson lines. For any given configuration (i.e. Metropolis time t), we compute the eigenvalues λ_1 and λ_2 of the Wilson lines $\mathbf{L}$ at each lattice site. We introduce their difference and average

$$\begin{aligned}\rho_1(t,\boldsymbol{x}) &= \tfrac{1}{2}|\lambda_1(t,\boldsymbol{x}) - \lambda_2(t,\boldsymbol{x})|,\\ \rho_2(t,\boldsymbol{x}) &= \tfrac{1}{2}|\lambda_1(t,\boldsymbol{x}) + \lambda_2(t,\boldsymbol{x})|.\end{aligned} \tag{37}$$

The ensemble of $\rho_1(t,\boldsymbol{x})$ defines its probability distribution $P_1(\rho_1)$, and similarly for $P_2(\rho_2)$. These can be turned into effective potentials for the sum and difference of eigenvalues, respectively, via

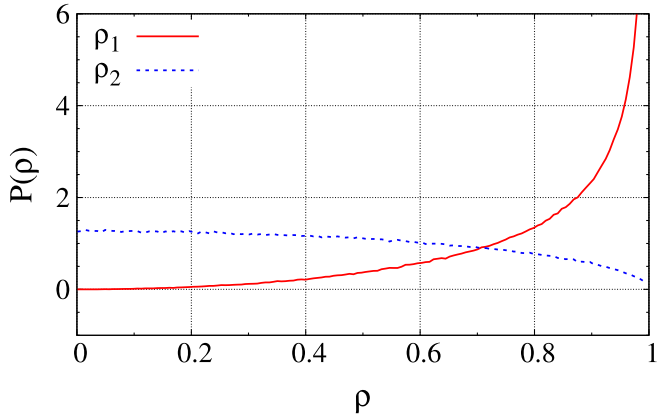

FIG. 6 (color online). The probability distributions of the difference (ρ_1) and sum (ρ_2) of eigenvalues of the Wilson line for $\beta = 1$ obtained on a $N_s = 48$ lattice.

$$V_{\text{eff}}(\rho_1) = -\log P_1(\rho_1), \qquad V_{\text{eff}}(\rho_2) = -\log P_2(\rho_2). \tag{38}$$

Figures 6 and 7 depict the probability distributions $P(\rho_1)$, $P(\rho_2)$, and the corresponding effective potentials for $\beta = 1$. We have also determined these quantities below the transition ($\beta = 0.5$) but obtained very similar curves. The potential shows evidence for a logarithmic divergence at $\rho_1 \to 0$ (or $\rho_2 \to 1$); this is expected as the group integration measure leads to logarithmic repulsion of the eigenvalues, compare to Eqs. (19) and (20). Aside from the effects of the Vandermonde determinant, however, the eigenvalue distribution (or the potential) for $\rho_2 \equiv (1/2)|\text{tr}\mathbf{L}|$ is entirely flat. This is illustrated in Fig. 7, which compares the pure Vandermonde potential $\log(1-\rho_2^2)^{-1/2}$ with the actually measured $V(\rho_2)$. The flat eigenvalue distribution is consistent with the free global rotations of $\bar{\mathbf{L}}$ observed above.

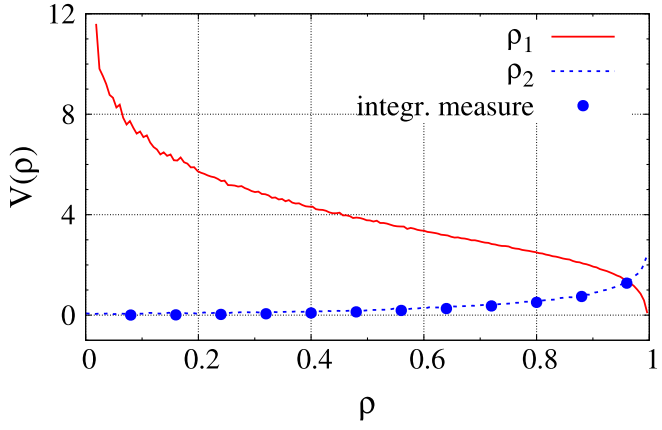

FIG. 7 (color online). The effective potentials for the difference (ρ_1) and sum (ρ_2) of eigenvalues of the Wilson line for $\beta = 1$ obtained on a $N_s = 48$ lattice. The pure integration measure in terms of ρ_2, which is given by $\log(1-\rho_2^2)^{-1/2}$, is shown by the points.

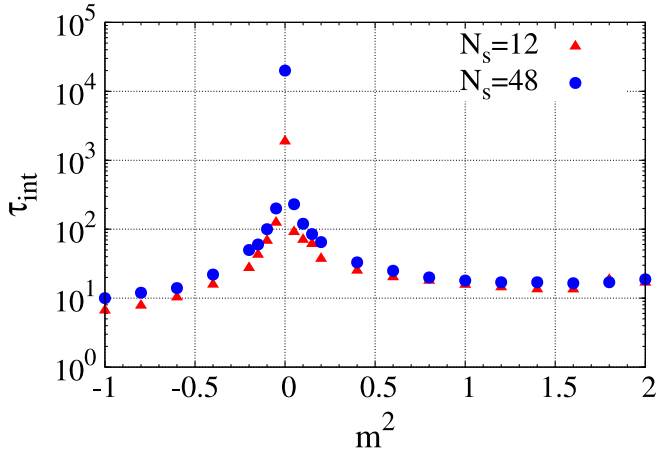

FIG. 8 (color online). The integrated autocorrelation time at $\beta = 1$ as a function of the coupling m^2 for various lattices.

B. Action with SU(2) symmetry

In this section, we add a mass term for the Polyakov loop $\ell = \text{tr}\mathbf{L}/2$,

$$\mathcal{S} = -\frac{1}{2}\beta\sum_{\langle ij\rangle}\text{tr}(\mathbf{L}_i\mathbf{L}_j^\dagger + \text{H.c.}) - m^2\sum_i|\text{tr}\mathbf{L}_i|^2, \tag{39}$$

which explicitly breaks $\text{SU}_L(2)\times\text{SU}_R(2)$ to SU(2), $\mathbf{L}\to\mathbf{\Omega}^\dagger\mathbf{L}\mathbf{\Omega}$, and also respects the $Z(2)$ symmetry for the Polyakov loop, $\ell\to-\ell$. We study the phase structure as a function of m^2 at fixed β. The order parameter for the deconfining phase transition is given by the ensemble and volume-averaged Polyakov loop $\langle|\bar{\ell}|\rangle = \langle|\text{tr}\bar{\mathbf{L}}/2|\rangle$, where $\bar{\mathbf{L}}$ is defined in Eq. (26).[5] In this section, $\langle|\bar{\ell}|\rangle$ will also be denoted as ℓ_0.

In Fig. 8, we show the integrated autocorrelation time for the Polyakov loop in the model (39) at $\beta = 1$ as a function of m^2. It indicates that the transition occurs in the vicinity of $m^2 \simeq 0$, where τ_{int} grows with the lattice volume (critical slowing down). However, contrary to Fig. 1, above the transition point τ_{int} is independent of the volume. This confirms to our expectation that long-range correlations in Metropolis time should not appear for $m^2 \neq 0$. A fit of the form $\tau_{\text{int}} \sim N_s^{1/\nu_\tau}$ to the $N_s = 24, 36, 48$ data gives

$$\nu_\tau = 1.3(4) \tag{40}$$

at $m^2 = 0$. As before, all subsequent measurements were performed with configurations that were separated by a time interval of τ_{int} (at least).

Figures 9 and 10 show the expectation value of the Polyakov loop, and its derivative with respect to the coupling, in a narrow window about the deconfining phase transition. Within errors, we find that the critical coupling is

[5]Taking the absolute value of $\bar{\ell}$ before performing the ensemble average is required due to the $Z(2)$ symmetry.

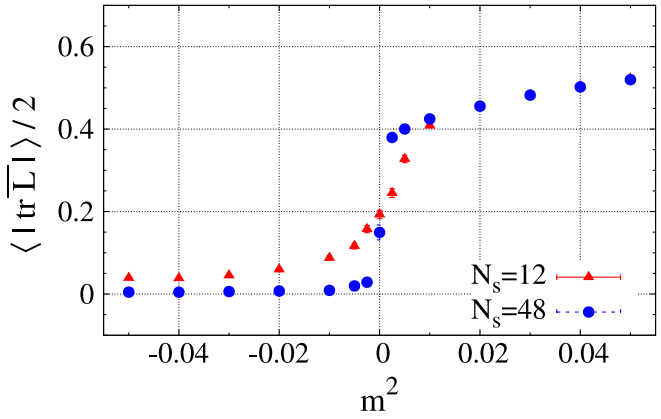

FIG. 9 (color online). The expectation value of the Polyakov loop as a function of the coupling m^2 (at $\beta = 1$) for various lattices.

$$m_c^2 = 0.000(2). \tag{41}$$

The transition in terms of m^2 is evidently rather sharp. Nevertheless, the scaling of $\tau_{\rm int}$ with the lattice size mentioned above suggests a second-order phase transition in infinite volume. This is confirmed also by the behavior of the inverse correlation length $m_\xi(m^2)$ shown in Fig. 11. m_ξ has been determined by the same procedure outlined in Eqs. (32) and (33), from the previous section, and appears to vanish at $m^2 = 0$, $N_s \to \infty$; fitting $m_\xi \sim N_s^{-1/\nu_\xi}$ (to the $N_s = 24, 36, 48$ data) gives the scaling exponent

$$\nu_\xi = 2.28(8). \tag{42}$$

In the deconfined phase at $m^2 > 0$, the correlation length decreases rapidly to about one (in lattice units). It decreases also as one goes to negative values of m^2, into the confined phase, but less rapidly. There, a weak volume dependence remains even from $N_s = 36$ to $N_s = 48$.

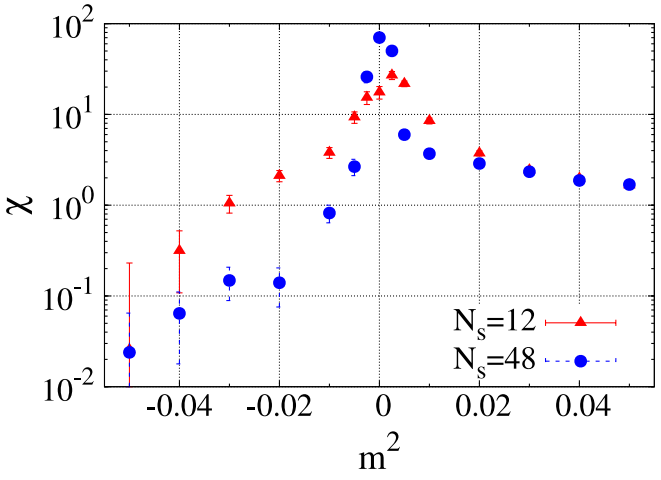

FIG. 10 (color online). The derivative of the Polyakov loop with respect to m^2 as a function of the coupling m^2 (at $\beta = 1$) on various lattices.

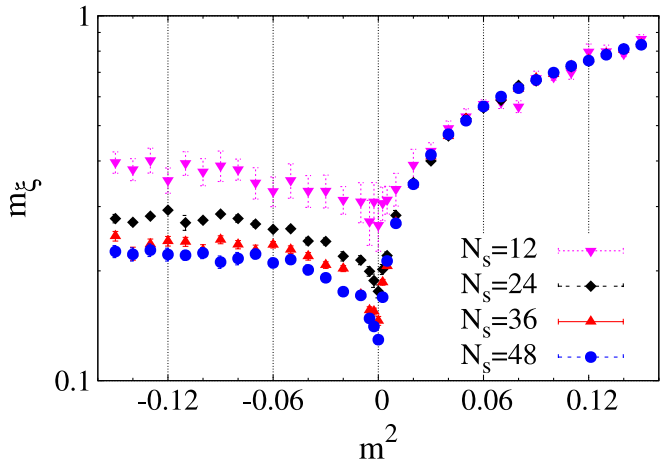

FIG. 11 (color online). The inverse spatial correlation length as a function of the coupling m^2 (at $\beta = 1$) for various lattices.

The expectation value of the Polyakov loop is shown again in Fig. 12 over a broader range of m^2. We also compare with the mean-field prediction (only for $\beta = 1$) discussed in Sec. III, which has been shifted to the right by $\Delta m^2 = 0.94$ to match the data far above the transition. Such a shift is expected by analogy to the tadpole contribution in a scalar theory, for example. Not surprisingly, mean-field theory works well for large $|m^2| \gtrsim 0.5$ (far from the transition, to both sides), when the effective masses are large and fluctuations are suppressed. Close to the phase transition, critical fluctuations invalidate the mean-field approximation.

The transition becomes extremely sharp when β is large, switching almost instantly from the confined phase to a perturbative deconfined phase with $\ell_0 \simeq 1$. This behavior is in line with the discussion in Secs. I and II: positive m^2 and

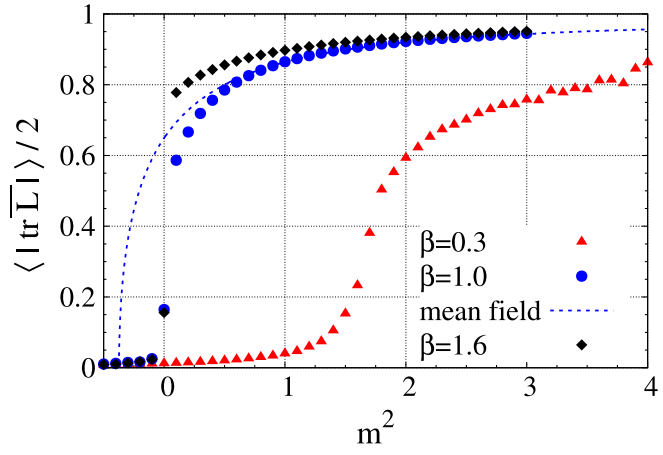

FIG. 12 (color online). The expectation value of the Polyakov loop as a function of the coupling m^2 at various β. Monte Carlo results obtained on a $N_s = 12$ lattice are indicated by the symbols. The line indicates the mean-field prediction for $\beta = 1$, shifted horizontally by $m_{\rm mf}^2 = m^2 - 0.94$.

large β corresponds to the weak-coupling limit of the four-dimensional theory in the deconfined phase. It can also be readily understood from the expression (39) for the action: at large β the Wilson lines at neighboring sites are forced to align such that $\mathrm{tr}\mathbf{L}_i\mathbf{L}_j^\dagger/2 \approx 1$. The potential only determines the direction of alignment: when $m^2 > 0$, the preferred direction is the unit matrix (eigenvalue attraction); when $m^2 < 0$, the Wilson lines instead live in the subspace spanned by the Pauli matrices (eigenvalue repulsion).

Figure 12 also shows that the deconfining phase transition is shifted to $m^2 > 0$ when $\beta < \beta_c$. In this limit, the alignment of the Wilson lines is enforced by the upside-down potential rather than the nearest-neighbor interaction.

Figure 13 depicts the eigenvalue distribution at $\beta = 1$ and $m^2 = 0.15$, which exceeds the critical m_c^2 for deconfinement (since $\ell_0 \simeq 0.6$) but is still far from asymptotic. Here, the perturbative potential (6) is partly cancelled by the fuzzy-bag term (7) and the eigenvalue distributions are rather broad. This result demonstrates that the fuzzy-bag term can generate eigenvalue repulsion in the deconfined phase, in the regime $\beta \approx \beta_c$ corresponding to moderately weak coupling in the underlying four-dimensional theory.

In the confined phase at $m^2 < 0$ and $\beta > \beta_c$, the Wilson lines fluctuate about the nontrivial vacuum $\mathbf{L}_c = i\tau_3$, or SU(2) rotations thereof [1,17,26]; this was shown in Fig. 6 already. As expected, the fluctuations diminish with increasing β, see Fig. 14. They are visible mostly in the distribution of the average eigenvalue ρ_2, while $P(\rho_1)$ is rather sharp. This can be understood easily by parameterizing the fluctuations about $i\tau_3$, as $\mathbf{L} \sim i\,\mathrm{diag}(e^{i\phi}, -e^{-i\phi})$, with $\phi \approx 0$. Then,

$$\rho_1 = |\cos\phi| \simeq 1 - \frac{\phi^2}{2}, \tag{43}$$

$$\rho_2 = |\sin\phi| \simeq |\phi|. \tag{44}$$

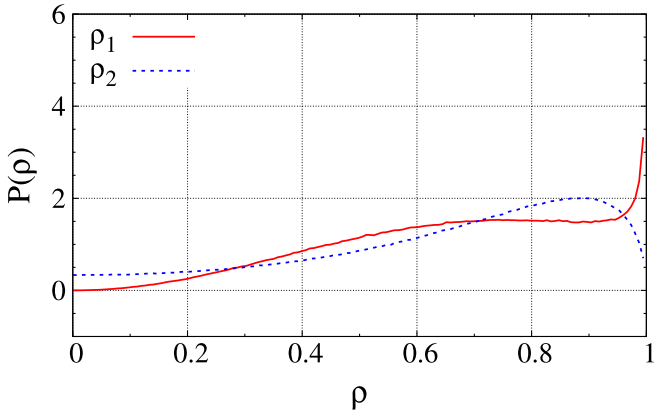

FIG. 13 (color online). Eigenvalue distributions for $m^2 = 0.15$ and $\beta = 1$; $N_s = 48$ lattice.

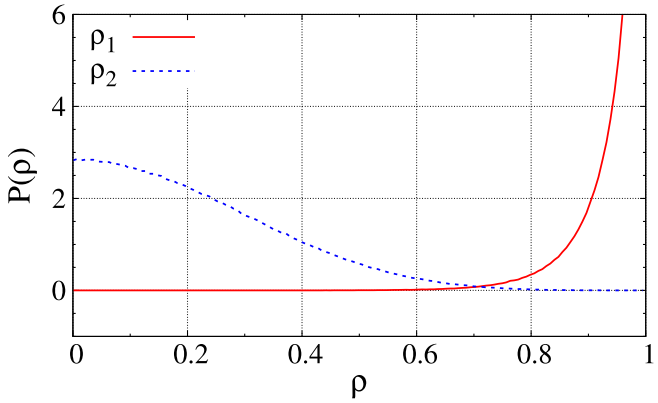

FIG. 14 (color online). Eigenvalue distributions for $m^2 = -0.05$ and $\beta = 3$; $N_s = 48$ lattice.

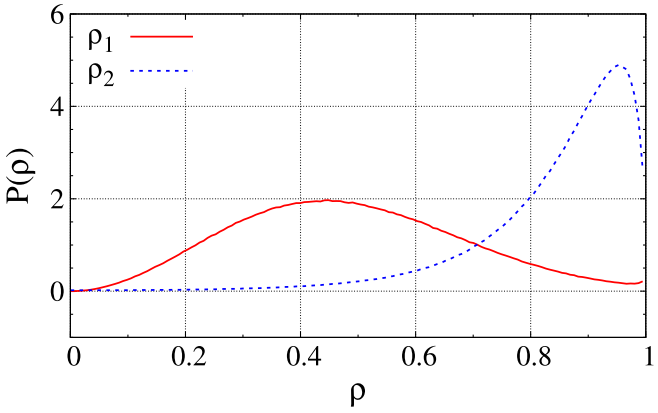

FIG. 15 (color online). Eigenvalue distributions for $m^2 = 0.8$ and $\beta = 1$; $N_s = 48$ lattice.

For large m^2 one of course approaches the perturbative vacuum, as shown in Fig. 15. The distribution for $\rho_2 = |\ell|$ peaks near 1, while that for the difference of eigenvalues is broader. In the perturbative regime, fluctuations can be parameterized as $\mathbf{L} \sim \mathrm{diag}(\exp i\phi, \exp -i\phi)$, with $\phi \approx 0$. Hence, the fluctuations of $\rho_1 = |\sin\phi|$ are much bigger than those of $\rho_2 = |\cos\phi| \simeq 1 - \phi^2/2$. The fact that $P(\rho_1) \to 0$ as $\rho_1 \to 0$, and $P(\rho_2) \to 0$ as $\rho_2 \to 1$, is again due to the integration measure, see Eq. (19). For even larger m^2, both distributions get sharper, and their maxima move further toward $\rho_1 = 0$ and $\rho_2 = 1$, respectively. In all, far above the transition the eigenvalue distributions qualitatively exhibit the behavior appropriate for the perturbative weak-field regime.

V. SUMMARY AND CONCLUSIONS

We have performed Monte Carlo simulations of an effective theory of SU(2) Wilson lines in three dimensions. The main purpose of this work was a study of eigenvalue repulsion in the deconfined phase of a SU(2) matrix model. We considered the action

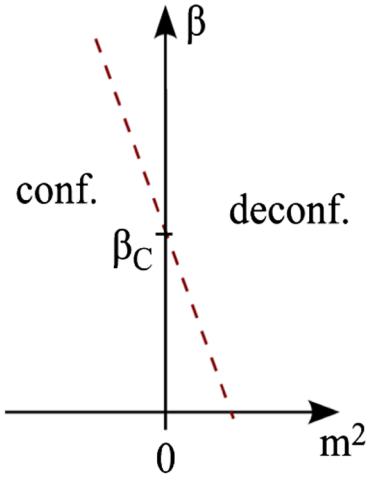

FIG. 16 (color online). Schematic sketch of the phase diagram in the $\beta - m^2$ plane, for infinite volume. The presence of an infinitesimal background field $-h\,\mathrm{tr}\mathbf{L}$ is assumed.

$$\mathcal{S} = -\frac{1}{2}\beta\sum_{\langle ij\rangle}\mathrm{tr}(\mathbf{L}_i\mathbf{L}_j^\dagger + \mathrm{H.c.}) - m^2\sum_i|\mathrm{tr}\mathbf{L}_i|^2, \qquad (45)$$

without gauge fields $A_i^a = 0$. The kinetic term exhibits a global $\mathrm{SU}_L(2) \times \mathrm{SU}_R(2)$ symmetry, which is broken explicitly to SU(2) by the loop potential. Note that a $\mathbf{L} \to \mathbf{\Omega}_L\mathbf{L}\mathbf{\Omega}_R$ transformation changes the eigenvalues of $\mathbf{L}$, while $\mathbf{L} \to \mathbf{\Omega}^\dagger\mathbf{L}\mathbf{\Omega}$ does not.

The phase diagram is sketched in Fig. 16. In the absence of a potential, at $m^2 = 0$, (45) is essentially a standard spin-model. At small β, the effective mass of the Wilson lines is large, and they fluctuate independently from site to site. Confinement is realized in a trivial way, since $\bar{\mathbf{L}} \to 0$ for each configuration, where $\bar{\mathbf{L}}$ denotes the volume-averaged Wilson line. This remains true for small $|m^2|$. To deconfine, a large upside-down potential ($m^2 > 0$) is required to align the Wilson lines to the unit matrix. Hence, for small β the phase transition arises due to the effective loop potential, in a regime where $\mathrm{SU}_L(2) \times \mathrm{SU}_R(2)$ is broken strongly.

There is a second-order phase transition at $\beta_c \simeq 0.942$ (and $m^2 = 0$), where the masses (inverse correlation lengths) of the Polyakov loop $\ell = \mathrm{tr}\mathbf{L}/2$ and of the adjoint fields $\tilde{\ell}^a = -i\,\mathrm{tr}\mathbf{L}\boldsymbol{\tau}^a/2$ vanish. This is associated with spontaneous breaking of $\mathrm{SU}_L(2) \times \mathrm{SU}_R(2)$ to SU(2), where three Goldstone modes appear. We have confirmed that the length $u^2 = \mathrm{tr}\bar{\mathbf{L}}^\dagger\bar{\mathbf{L}}/2$ of $\bar{\mathbf{L}}$ aquires a nonzero expectation value for $\beta > \beta_c$. Hence, we expect that a weak background field $-h\,\mathrm{tr}\mathbf{L}$, $h \to 0$, shifts the phase boundary to $m^2 < 0$ as indicated in Fig. 16.

Very large lattice coupling $\beta \gg 1$ corresponds to the extreme weak-coupling limit of the original four-dimensional theory; the effective theory can nevertheless confine, because it incorporates the global $Z(N)$ symmetry for the Polyakov loop. At large β, fluctuations are suppressed, and the Wilson lines are again forced to align, this time by the nearest-neighbor interaction (kinetic term). The direction of alignment is determined by the loop potential. A standard potential with positive curvature ($m^2 < 0$) is minimized by Wilson lines with no singlet component, hence, eigenvalues repel, and the theory confines.[6] On the other hand, an upside-down potential ($m^2 > 0$) leads to $\mathbf{L}(\boldsymbol{x}) \sim \mathbb{1}$ and so to eigenvalue attraction and deconfinement. For $\beta \gg 1$ even a weak potential suffices to trigger the locking into (or out of) the center of the group. This leads to a sharp transition directly to a perturbative deconfined phase without eigenvalue repulsion.

We have measured the distributions of the eigenvalues of the Wilson line in the nonperturbative deconfined phase above, but close to β_c. They show clearly the emergence of eigenvalue repulsion even for "temperatures" (i.e. m^2) not extremely close to the phase boundary. It is only relatively deep in the deconfined phase ($m^2 \gtrsim 1$) that the distribution of eigenvalues peaks near 1, which corresponds to the perturbative vacuum. These results confirm the suggestion of Ref. [1] that eigenvalue repulsion in the deconfined phase does arise at intermediate values of the nearest-neighbor coupling β, due to fluctuations of the Wilson lines, provided that the nonperturbative fuzzy-bag term approximately cancels the perturbative loop potential. Such a fuzzy-bag contribution in the effective theory makes it possible to reach the region of small m^2 in the phase diagram.

In the confined phase at $\beta > \beta_c$, the volume-averaged Wilson line $\bar{\mathbf{L}}$ approaches the center-symmetric vacuum [1,17,26]

$$\mathbf{L}_c = \mathrm{diag}(1, z, z^2, \cdots, z^{N-1}), \qquad (z \equiv e^{2\pi i/N}), \qquad (46)$$

which for two colors corresponds to $\mathbf{L}_c = i\tau_3$ (up to an overall SU(2) rotation). This is due to the fact that the Wilson lines align at large β, and $m^2 < 0$ favors a direction orthogonal to unity. We repeat that this is not the case when β is small, where instead $\bar{\mathbf{L}} \to 0$ for $m^2 \simeq 0$.

ACKNOWLEDGMENTS

We are indebted to Rob Pisarski for many helpful discussions. D. S. gratefully acknowledges support from the Helmholtz foundation. The numerical simulations presented here were performed at the Center for Scientific Computing at Frankfurt University. Our code is based in part on the MILC Collaboration's public lattice gauge theory code, see [27].

[6]We expect that the phase boundary is shifted from $m^2 = 0$ to some smaller value, if an infinitesimal background field is applied.

[1] R. D. Pisarski, Phys. Rev. D **74**, 121703(R) (2006).
[2] A. Vuorinen and L. G. Yaffe, Phys. Rev. D **74**, 025011 (2006).
[3] O. Kaczmarek, F. Karsch, P. Petreczky, and F. Zantow, Phys. Lett. B **543**, 41 (2002); S. Gupta, K. Hübner, and O. Kaczmarek, Nucl. Phys. **A785**, 278 (2007); O. Kaczmarek, S. Gupta, and K. Hübner, Proc. Sci. LAT2007 (2007) 195 [arXiv:0710.2277]; S. Gupta, K. Hübner, and O. Kaczmarek, arXiv:0711.2251.
[4] A. Dumitru, Y. Hatta, J. Lenaghan, K. Orginos, and R. D. Pisarski, Phys. Rev. D **70**, 034511 (2004).
[5] L. D. McLerran and B. Svetitsky, Phys. Lett. **98B**, 195 (1981).
[6] D. Diakonov and M. Oswald, Phys. Rev. D **68**, 025012 (2003); **70**, 105016 (2004).
[7] J. Engels, J. Fingberg, K. Redlich, H. Satz, and M. Weber, Z. Phys. C **42**, 341 (1989); J. Engels, F. Karsch, and K. Redlich, Nucl. Phys. **B435**, 295 (1995); J. Engels, S. Mashkevich, T. Scheideler, and G. Zinovev, Phys. Lett. B **365**, 219 (1996).
[8] A. Velytsky, arXiv:0711.0748.
[9] B. Svetitsky and L. G. Yaffe, Nucl. Phys. **B210**, 423 (1982).
[10] G. Boyd, J. Engels, F. Karsch, E. Laermann, C. Legeland, M. Lutgemeier, and B. Petersson, Nucl. Phys. **B469**, 419 (1996).
[11] A. Dumitru and R. D. Pisarski, Phys. Rev. D **66**, 096003 (2002); R. Falcone, R. Fiore, M. Gravina, and A. Papa, Nucl. Phys. **B785**, 19 (2007).
[12] See, for example, J. O. Andersen and M. Strickland, Ann. Phys. (N.Y.) **317**, 281 (2005); Y. Schröder, Proc. Sci. JHW2005 (2006) 029; J. P. Blaizot, Nucl. Phys. A **785**, 1 (2007), and references therein.
[13] Ph. de Forcrand, A. Kurkela, and A. Vuorinen, arXiv:0801.1566.
[14] R. D. Pisarski, Phys. Rev. D **62**, 111501 (2000).
[15] A. Dumitru, J. Lenaghan, and R. D. Pisarski, Phys. Rev. D **71**, 074004 (2005).
[16] D. J. Gross, R. D. Pisarski, and L. G. Yaffe, Rev. Mod. Phys. **53**, 43 (1981).
[17] P. N. Meisinger, T. R. Miller, and M. C. Ogilvie, Phys. Rev. D **65**, 034009 (2002); P. N. Meisinger, M. C. Ogilvie, and T. R. Miller, Phys. Lett. B **585**, 149 (2004).
[18] E. Megias, E. Ruiz Arriola, and L. L. Salcedo, J. High Energy Phys. 01 (2006) 073.
[19] A. Kurkela, Phys. Rev. D **76**, 094507 (2007).
[20] J. B. Kogut, M. Snow, and M. Stone, Nucl. Phys. **B200**, 211 (1982).
[21] P. H. Damgaard, Phys. Lett. B **194**, 107 (1987); J. Christensen and P. H. Damgaard, Phys. Rev. Lett. **65**, 2495 (1990); Nucl. Phys. **B348**, 226 (1991); **B354**, 339 (1991).
[22] See, for example, B. Svetitsky, Phys. Rep. **132**, 1 (1986).
[23] L. Dittmann, T. Heinzl, and A. Wipf, J. High Energy Phys. 06 (2004) 005; T. Heinzl, T. Kaestner, and A. Wipf, Phys. Rev. D **72**, 065005 (2005); C. Wozar, T. Kaestner, A. Wipf, T. Heinzl, and B. Pozsgay, Phys. Rev. D **74**, 114501 (2006).
[24] R. D. Pisarski, arXiv:hep-ph/0203271.
[25] B. A. Berg, *Markov Chain Monte Carlo Simulations and Their Statistical Analysis* (World Scientific, Singapore, 2004).
[26] M. Schaden, Phys. Rev. D **71**, 105012 (2005).
[27] For MILC collaboration's public lattice gauge theory code, see http://physics.utah.edu/~detar/milc.html